A&A 585, A131 (2016)
DOI: 10.1051/0004-6361/201527281

Astronomy & Astrophysics

The spectrum of Pluto, 0.40–0.93 μm

I. Secular and longitudinal distribution of ices and complex organics

V. Lorenzi[1], N. Pinilla-Alonso[2], J. Licandro[3,4], D. P. Cruikshank[5], W. M. Grundy[6], R. P. Binzel[7], and J. P. Emery[2]

[1] Fundación Galileo Galilei-INAF, Rambla José Ana Fernández Pérez, 7, 38712 Breña Baja, TF, Spain
e-mail: lorenzi@tng.iac.es
[2] Department of Earth and Planetary Sciences, University of Tennessee, 1412 Circle Drive, Knoxville, TN 37996, USA
[3] Instituto Astrofísico de Canarias, IAC, C/ vía Láctea, s/n, 38205 La Laguna, TF, Spain
[4] Departamento de Astrofísica, Universidad de La Laguna, Avenida Astrofísico Francisco Sánchez, s/n, 38200 La Laguna, TF, Spain
[5] NASA Ames Research Center, Moffett Field, CA 94035, USA
[6] Lowell Observatory, 1400 W Mars Hill Rd, Flagstaff, AZ 86001, USA
[7] Massachusetts Institute of Technology, 77 Massachusetts Ave, Cambridge, MA 02139, USA

Received 31 August 2015 / Accepted 23 November 2015

ABSTRACT

Context. During the past 30 years the surface of Pluto has been characterized and its variability monitored through continuous near-infrared spectroscopic observations. But in the visible range only a few data are available.
Aims. The aim of this work is to define Pluto's relative reflectance in the visible range to characterize the different components of its surface, and to provide ground based observations in support of the New Horizons mission.
Methods. We observed Pluto on six nights between May and July 2014 with the imager/spectrograph ACAM at the *William Herschel* Telescope (La Palma, Spain). The six spectra obtained cover a whole rotation of Pluto ($P_{\rm rot}$ = 6.4 days). For all the spectra, we computed the spectral slope and the depth of the absorption bands of methane ice between 0.62 and 0.90 μm. To search for shifts in the center of the methane bands, which are associated with dilution of CH_4 in N_2, we compared the bands with reflectances of pure methane ice.
Results. All the new spectra show the methane ice absorption bands between 0.62 and 0.90 μm. Computation of the depth of the band at 0.62 μm in the new spectra of Pluto and in the spectra of Makemake and Eris from the literature, allowed us to estimate the Lambert coefficient at this wavelength at temperatures of 30 K and 40 K, which has never been measured before. All the detected bands are blueshifted with respect to the position for pure methane ice, with minimum shifts correlated to the regions where the abundance of methane is higher. This could be indicative of a dilution of CH_4:N_2 that is more saturated in CH_4. The longitudinal and secular variations in the parameters measured in the spectra are in accordance with results previously reported in the literature and with the distribution of the dark and bright materials that show the Pluto's color maps from New Horizons.

Key words. Kuiper belt objects: individual: Pluto – methods: observational – methods: numerical – techniques: spectroscopic

1. Introduction

The surface of Pluto is covered with ices of varying degrees of volatility, and even at its low average temperature of ~40 K, there is an exchange of molecules between the surface and the thin atmosphere. Because of Pluto's high obliquity (119.6°) and the eccentricity of its orbit (perihelion 29.66 AU, aphelion 48.87 AU), there are pronounced seasons over the 247.7-year orbital period. These factors ensure that Pluto's surface undergoes changes on a seasonal time scale. Secular changes may also occur, owing to the long-term evolution of the chemical components of the surface and atmosphere under the influence of solar and cosmic ray irradiation. On the time scale of Pluto's 6.4-day rotation period, clear changes in the distribution of ices across its surface are seen.

Indeed, on secular and rotational time scales, changes in Pluto's overall (global) brightness and in the near-infrared spectral signatures of the three principal ices, N_2, CH_4, and CO have been detected and quantified (Grundy et al. 2013, hereafter G13; Cruikshank et al. 2015, and references therein). Because Pluto has only been observed over one-third of its full orbit, secular changes might be confused with seasonal variations, with the result that at the present time, there is no unequivocal evidence of any observable secular changes.

In addition to the ices on Pluto' surface, there is another material present that imparts colors as seen in the extended visible spectral region, 0.30–1.00 μm. As deduced from multi-color photometric measurements and images, the colors vary from light to medium yellow, red-brown, to black (Buie et al. 2010b). The ices detected to date do not produce these colors, and it is generally accepted that photochemical reactions in Pluto's atmosphere and in the surface ices create colored macromolecular matter that contains or is made of complex organic chemicals derived from carbon, nitrogen, and oxygen (e.g., Materese et al. 2014). The coloring properties of these materials are well established (e.g., Khare et al. 1984; Cruikshank et al. 2005; Imanaka et al. 2012; Materese et al. 2014). The coloring agent is not uniform over Pluto's surface, changing noticeably over the dwarf-planet's 6.4-day rotation.

The best way to quantify the color of Pluto and to search for diagnostic characteristics is to record the reflectance properties of the surface in the photovisual or extended visual spectral

Table 1. Details of the observations.

2014 date	Time	am (Pluto)	Solar analog	am (SA)	Lon (deg)	Lat (deg)	p_v
May 13	04:38	1.5	L112-1333	1.6	103.7°	51.2°	0.44
			L107-684	2.3			
May 14	03:40	1.6	L112-1333	1.7	49.7°	51.2°	0.48
			L107-684	1.5			
June 6	01:50	1.7	L112-1333	1.5	197.9°	50.9°	0.59
			L107-684	1.2			
June 7	01:57	1.6	L112-1333	1.5	141.3°	50.9°	0.50
			L107-684	1.3			
June 18	00:23	1.8	L112-1333	2.3	245.2°	50.7°	0.57
			P041C	1.5			
July 17	22:40	1.7	L112-1333	1.7	358.9°	50.0°	0.52
			P041C	1.4			

Notes. Time = mid exposure time; am (Pluto) and am (SA) = mid exposure airmass of Pluto and the solar analogs, respectively; Lon = Pluto sub-Earth longitude; Lat = Pluto sub-Earth latitude; p_v = Geometric albedo of Pluto at 0.56 μm.

region (0.30–1.00 μm). Only a few such measurements have been reported in the literature, beginning with observations made in 1970 by Fix et al. (1970) and followed by Benner et al. (1978), Bell et al. (1979) (data published in Cruikshank & Brown 1986), Barker et al. (1980), Buie & Fink (1987), and Grundy & Fink (1996). Individually or together, these studies do not define a well-sampled range of rotation and seasonal change or a full sample of wavelengths in the desired range at adequate spectral resolution. The history of color measurements with ground-based telescopes and the *Hubble* Space Telescope (HST) is reviewed by Cruikshank et al. (2015), who note that the color measured in the $(B-V)$ photometric index was constant from 1953 to 2000 within a few tenths of a percent, but then changed abruptly in 2002. Buie et al. (2010b) give the details of the HST observations that showed a global change in color to a redder $(B-V)$ index that persists to the present day.

The variation in the relative amounts of ices and dark material have been mapped before (Buie et al. 2010b; G13), but are even more obvious now in light of the preliminary new images obtained by the New Horizons mission. The maps combining the reflectance and colors of Pluto's surface clearly show a diverse palette from the very dark region on the equator, informally named Cthulhu Regio to the "clear peach orange" region, informally named the Tombaugh Regio (Stern et al. 2015).

During 2014, we conducted a new observational study in order to provide a high-quality data set of spectrophotometric data in the 0.40–0.93 μm spectral range. These observations enable the definition of Pluto's reflectance and the investigation of weak methane ice absorption bands shortward of 1.00 μm. The data have hemispheric spatial resolution over a whole rotation of the Pluto's longitudes. The new data are compared with earlier observations to detect any changes in spectral reflectance that may have occurred in the past few decades. This comparison also provides a basis for modeling the spectrum with radiative transfer models that account for the known components of Pluto's surface, as well as additional components that are suspected to occur. The observations presented here include the reflected light of both Pluto and Charon. These observations are also in support of the New Horizons mission that observed the Pluto system in July 2015 and are part of a long-term campaign to follow the secular evolution of Pluto's surface properties.

In the next section we describe the observations. In Sect. 3 we analyze the obtained spectra: we calculate the slopes of the relative reflectances, we calculate the depth and the area of the absorption bands of methane ice, and we measure the shifts of their centers. In Sect. 4 we discuss the results, and in Sect. 5 we report our conclusions.

2. The observations

We observed Pluto on six different nights between May 13 and July 17, 2014 using the low-resolution spectroscopic mode of ACAM (auxiliary-port camera, Benn et al. 2008). ACAM is an imager/spectrograph that is mounted permanently at a folded-Cassegrain focus of the 4.2 m *William Herschel* Telescope at the Observatorio del Roque de los Muchachos (ORM), La Palma. We used the V400 disperser and the 1.5″ slit providing a resolution of ~300 at 0.55 μm (the dispersion is 3.3 Å/px). The slit was oriented at the parallactic angle, and the tracking of the telescope was set to compensate for Pluto's proper motion.

To cover a whole rotation of Pluto, we originally scheduled seven observations equally spaced in time to observe Pluto's surface every ~50 degrees in longitude. Unfortunately, we discarded one of those observations because of technical problems. The six that we kept cover 310 degrees in longitude. The details of the observations are described in Table 1. We define longitudes following the IAU2009 model that corresponds with the *right-hand rule*. Every night we obtained three consecutive spectra of Pluto of 300-second exposure times each, which provides a $S/N > 200$ in most of the wavelength range and even better after averaging the three spectra.

Data was reduced using the Image Reduction and Analysis Facility (IRAF) standard procedures (Tody 1993). Preprocessing of the CCD images included bias and flat field correction. Flat field images were obtained using calibration lamps (tungsten continuum lamp) in the afternoon. Wavelength-calibration lamps (CuAr and CuNe) were obtained before and after the set of Pluto's spectra, maintaining the same position angle to avoid the effect of instrumental flexures in the wavelength calibration.

To correct the spectra for telluric absorptions and to obtain the relative reflectance, we observed every night two different Landolt stars (Landolt 1992) that have proven to be good solar analogs (Licandro et al. 2003). We observed them at airmasses that are very similar to that of Pluto (see Table 1 for the details). These solar analogs are bright ($10 < V_{\rm mag} < 12.4$) so the exposure times were always shorter than 60 s. To reduce the number of bad pixels and artifacts, we obtained three spectra of each of the stars as we did for Pluto. The reduction of the spectra of the solar analogs was done following the same procedure as for

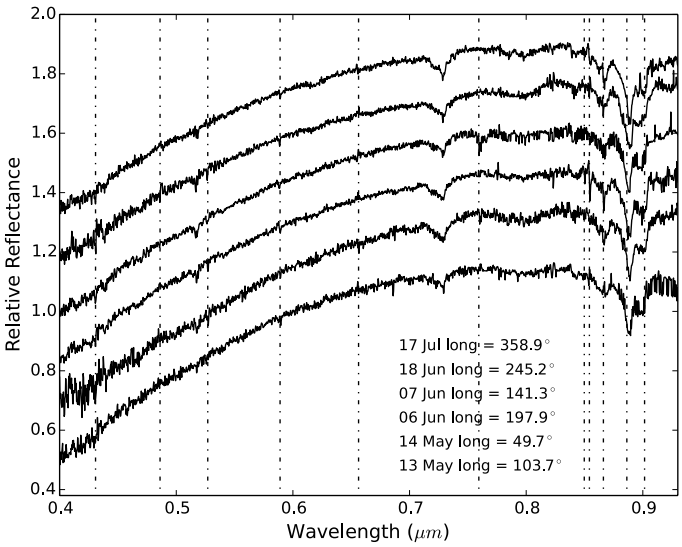

Fig. 1. Relative reflectances of Pluto corresponding to hemispheres centered on six different sub-Earth longitudes. All the reflectances are normalized at 0.60 μm and shifted by 0.15 in relative reflectance for clarity. The labels are ordered (top to bottom) in the same order as the reflectances. The vertical dashed lines show the telluric absorptions. Some of these telluric absorptions have not been completely removed. The absorption at 0.52 μm is an artifact and is present on the spectra of the solar analogs. Its center corresponds to the magnesium triplet (0.5169–0. 5183 μm) that is present in G stars.

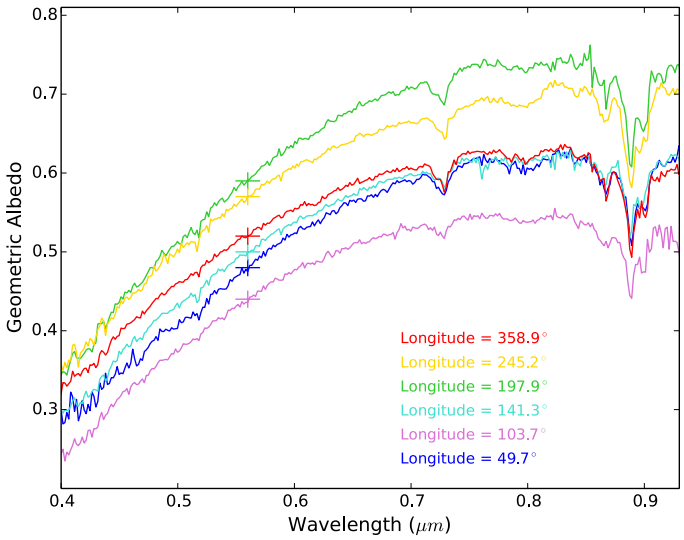

Fig. 2. Same spectra of Fig. 1 smoothed using an average filter of 5 pixels and represented in geometric albedo. The symbol plus indicates, for each spectrum, the global geometric albedo of Pluto alone at 0.56 μm calculated for the corresponding date of the observation.

Pluto. All the calibration images, the solar analogs, and the Pluto images were obtained in about one hour.

The extinction of the sky is dependent on the wavelength, with shorter wavelengths experience greater extinction. To minimize the spectral extinction effect from the difference in airmass between the stars and the target, we applied color correction to the spectra of the object and the stars. We used the mean extinction coefficient for the Observatorio del Roque de los Muchachos (King 1985).

We finally divided the color-corrected spectra of Pluto by the color-corrected spectra of the stars to obtain Pluto's relative reflectance. We used the sky lines at this step to refine the wavelength calibration. Before averaging all of them into a "final" relative reflectance, we visually inspected the 18 reflectances for each night, obtained by dividing the three spectra of Pluto by the three spectra of each solar analog, and discarded those that showed problems due to the systematic errors (~20% of the total). We averaged the rest of them into a final relative reflectance for each date of observation.

In Fig. 1 we present the six reflectance spectra obtained in this observing campaign. These are the average of the Pluto + Charon spectra divided by the spectra of the solar-type stars. This division cancels the solar color and the solar and telluric absorption lines. The spectra have been normalized to 1.0 at 0.75 μm to enhance the differences in the slope of the continuum below 0.70 μm. The contribution of Charon has not been removed in this plot. Nevertheless, the spurious light of Charon is not a problem because Charon is two magnitudes fainter than Pluto, and its color is neutral at these wavelengths (as we explain in detail later).

In Fig. 2, we present the data from Fig. 1 smoothed using an average filter of five pixels and plotted in geometric albedo. To transform from reflectance to albedo, we used the magnitudes of Pluto alone from Fig. 1 of Buie et al. (2010a), in which they plot the lightcurve of Pluto resolved from Charon. The values in the figure are shown as mean opposition magnitudes corrected to phase angle $\alpha = 1°$. We have taken the Buie et al. (2010a) magnitudes at $\alpha = 1°$ for the longitudes we observed and have calculated the geometric albedos corresponding to those longitudes. Using a radius of 1184 km for the dwarf planet (Lellouch et al. 2015), we calculated the global geometric albedo of Pluto alone at the V wavelength (0.56 μm) for each date that we observed (listed in Table 1) using the equation

$$-2.5 \log p_V = V_{\rm Sun} - V_{\rm Pluto} - 5 \log r + 5 \log(R \times \Delta),$$

where $V_{\rm Sun} = -26.75$, r = Pluto's radius (in AU), R = Pluto's mean heliocentric distance (39.482 AU), and Δ = Pluto's geocentric distance (38.482 AU). A small revision of Pluto's radius from the New Horizons investigation makes a negligible change to the albedo calculations.

We made no correction for the contribution of Charon to the color of (Pluto + Charon) that we observed, assuming that Charon's color is neutral gray. From observations of the mutual transit and occultation events of the mid-1980s, Binzel (1988) found a nearly neutral gray color for Charon, with $B - V = 0.70 \pm 0.01$ ($(B - V)_{\rm Sun} = 0.65$). More recently, Buie et al. (2010a) have derived $(B-V) = 0.7315 \pm 0.0013$ using HST data. At the photometric B band (0.44 μm), Tholen & Buie (1990) give the geometric albedo of Pluto as 0.44–0.61 and 0.38 for Charon.

3. Results and analysis

For each spectra we computed four parameters: (1) the spectral slope in order to quantify the color of Pluto at different longitudes and, thus, search for possible variations in the amount of solid complex organics over its surface; (2) the integrated area of the absorption bands of methane ice at 0.62 μm in order to determine if this weak CH_4 band is detected as in other trans-Neptunian objects (TNOs; Licandro et al. 2006b; Alvarez-Candal et al. 2011); (3) the depth of the methane ice bands between 0.62 and 0.90 μm in order to search for possible variations in the abundance of CH_4-ice on the surface of Pluto with longitude; (4) the shift in the center of the absorption bands

of methane ice at 0.73, 0.79, 0.80, 0.84, 0.87, and 0.89 μm in order to search for possible variations in the dilution of CH_4 in N_2 with longitude (previously reported by Quirico & Schmitt 1997).

3.1. Slope

The slope in the visible is an indicator of the amount, particle size, or type of complex organics on the surface. Complex organics have been detected on the surface of asteroids (24) Themis and (65) Cybele (Rivkin & Emery 2010; Licandro et al. 2011) and the Saturnian moons Iapetus and Phoebe (Cruikshank et al. 2008, 2014), and their presence has been inferred for other solar system objects (e.g., TNOs and Titan, Cruikshank et al. 2005). Recently a suite of 16 organic compounds, comprising numerous carbon and nitrogen-rich molecules, has been discovered on the surface of the comet 67P/Churyomov-Gerasimenko (Wright et al. 2015; Goesmann et al. 2015). The comet presents a red slope in the visible range (between 5 and 25%/1000 Å, Capaccioni et al. 2015). This discovery suggests that organic compounds that are the precursors of the more complex organics (such as tholins) are a ubiquitous ingredient of the minor bodies in the solar system. Not surprisingly, red slopes, which are typically associated with the complex organics, are common among the spectra of TNOs.

Here we compute the slope of Pluto's visible spectrum in two ranges: from 0.40 to 0.70 μm and from 0.57 to 0.70 μm. The first range comprises the full spectral region below 0.70 μm covered by our spectra. The second range enables the comparison with previous spectra of Pluto, Eris, and Makemake from the literature. To compute the slope values in both cases, we first normalized all the spectra at 0.60 μm, and then we fit each of them in the chosen range with a linear function. We made this computation for all the six spectra and for the average relative reflectance. The slope is expressed here as %/1000 Å.

To evaluate the errors in the computation of the slope, we took both the error in the fit and the systematic errors in the reflectance into account. The systematic errors depend on different contributions: e.g., errors introduced by color corrections or by dividing by the spectra of the solar analogs. The error introduced by dividing by the spectra of the solar analog is the dominant part of the systematic errors. To estimate this error, we compared the six individual spectra of the stars observed each night following the procedure described in Lorenzi et al. (2014) and Pinilla-Alonso (2016). After discarding those spectra displaying extreme behavior, we took the standard deviation of the slope of these spectra as the error in the slope for the night. These values are shown in Table 2. We took the maximum value in the run as the systematic error. We found that the formal error coming directly from the computation of the slope is an order of magnitude lower than the systematic error, so we took 0.8%/1000 Å as the final uncertainty associated to the slope calculation for all the spectra.

In any case, it is important to notice that the spectra presented in this paper are the spectra of the Pluto-Charon system. Even if the spectrum of Charon is flat in the visible wavelength range, so does not affect the measurements of the methane bands that are only due to Pluto spectrum, the spectral slope of the Pluto only spectrum will be slightly redder. In fact, if we consider that the spectral slope of Pluto+Charon S'_{P+C}, calculated for example between 0.40 and 0.70 μm for a spectrum normalized at 0.60 μm, is

$$S'_{P+C} = \left[\frac{F_{P+C}(0.70)}{F_{\odot}(0.70)} - \frac{F_{P+C}(0.40)}{F_{\odot}(0.40)}\right] \times \frac{F_{\odot}(0.60)}{F_{\odot}(0.60)},$$

Table 2. Estimated systematic error in the slope expressed in %/1000 Å.

2014 date	Syst. error	2014 date	Syst. error
May 13	0.45	June 7	0.76
May 14	0.70	June 18	0.73
June 6	0.37	July 17	0.71

where $F_{P+C}(X)$ and $F_{\odot}(X)$ are the flux of Pluto+Charon and the flux of the Sun at X μm, respectively, and assuming that

$$\frac{F_C(0.40)}{F_{\odot}(0.40)} = \frac{F_C(0.60)}{F_{\odot}(0.60)}$$

(because Charon's spectral slope in the visible is close to 0), we find that the slope of Pluto alone S'_P, is

$$S'_P = \frac{F_{P+C}(0.60)}{F_P(0.60)} \times S'_{P+C}.$$

Considering the albedo and size of Pluto and Charon and the albedo dependence with wavelength (in particular, the dependence of Pluto's albedo in the visible, as Charon's albedo in the visible is almost constant), we find that the spectral slope of the Pluto-only spectrum is between 11% and 14% larger (e.g., in the 0.40–0.70 μm region, the average slope will be 21–22 %/1000 Å). We preferred not to correct for the Charon contribution to avoid introducing errors that are an artifact of the processing and to facilitate the comparison with past measurements. Nonetheless, for the scientific investigations within this paper, Charon's contribution is not a critical factor.

To compare with other spectra in the literature, we computed the slope of those spectra in the same way as we did for the new data presented herein. For this comparison, we used the spectra of Pluto from Grundy & Fink (1996) and the spectra of two other large TNOs, (136472) Makemake from Licandro et al. (2006a) and (136199) Eris from Alvarez-Candal et al. (2011). For the spectra from the literature of Pluto, Makemake, and Eris, there are no estimates for the systematic errors in the original papers, so we take the typical value of 1%/1000 Å (e.g., Lazzaro et al. 2004) for all the spectra. (For these spectra the systematic errors are also an order of magnitude greater than those associated with the fit calculation.) The results are listed in Table 3.

3.2. Methane absorption bands

The new spectra clearly show methane ice absorption bands at 0.73, 0.78–0.80, and 0.83–0.91 μm. In Fig. 3, we show the spectrum of Pluto obtained averaging the six spectra presented in this work, with the methane ice absorption bands evidenced as vertical dotted lines. All these bands have very low absorption coefficients, 5.0×10^{-2}, ~$1.3–1.4 \times 10^{-2}$, ~$1.0–8.0 \times 10^{-2}$ cm^{-1}, respectively, as measured in the laboratory at 40 K (Grundy et al. 2002). This average spectrum also shows an absorption around 0.62 μm. This band has been also observed in the spectra of other large TNOs dominated by methane ice, like Eris and Makemake (Alvarez-Candal et al. 2011; Licandro et al. 2006b, see Fig. 4), so its identification is not in question. However, the absorption coefficient of this band is unknown since it has not been measured in the laboratory. If we look at each particular reflectance obtained in 2014, some of them show it very clearly, in particularly the phase centered at 358.9°.

To confirm our detection, we compute the integrated area of the absorption band. For this computation, we first fit a

Table 3. Computed spectral slope between 0.57 and 0.70 μm and between 0.40 and 0.70 μm, with the spectra normalized at 0.60 μm, for the spectra of Pluto+Charon (this work; Buie & Fink 1987; Grundy & Fink 1996), for the spectrum of Makemake (Licandro et al. 2006b) and for the spectrum of Eris (Alvarez-Candal et al. 2011).

Longitude (degrees)	Slope (%/1000 Å) 0.57–0.70 μm	Slope (%/1000 Å) 0.40–0.70 μm	Reference
49.7°	14.2	19.9	This work
103.7°	12.6	20.6	″
141.3°	12.5	19.3	″
197.9°	12.7	19.4	″
245.2°	10.7	17.3	″
358.9°	10.8	17.2	″
Average spectrum	12.3	19.0	″
25° (1983)	5.7	–	Buie & Fink (1987)
329° (1983)	5.1	–	″
144° (1990)	7.7	–	Grundy & Fink (1996)
56° (1993)	10.8	–	″
150° (1994)	10.4	–	″
Makemake	12.9	17.3	Licandro et al. (2006b)
Eris	4.4	6.5	Alvarez-Candal et al. (2011)

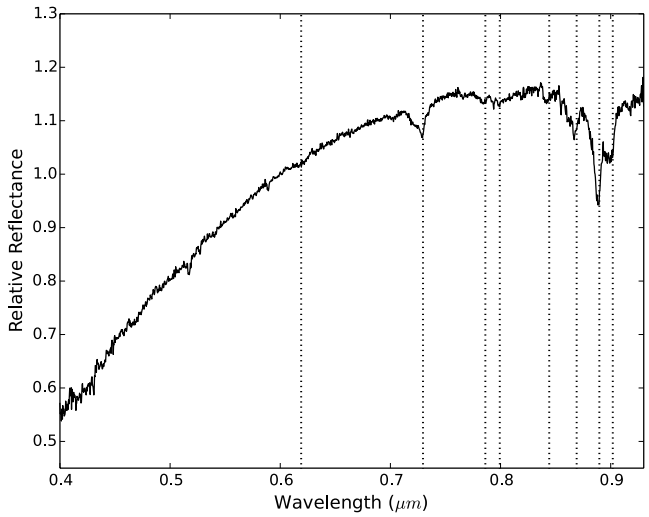

Fig. 3. Averaged spectrum of the six spectrum presented in this work, normalized at 0.60 μm. The positions of the absorption bands of CH_4 are represented by dotted lines. The features at 0.43, 0.52, and 0.59 μm are artifacts due to small differences between the spectra of the G2 stars used as solar analogs and those of the Sun. The 0.43 μm structure corresponds to the absorption produced by iron and calcium, the 0.52 μm is due to the magnesium triplet, and the 0.59 μm is due to a sodium doublet.

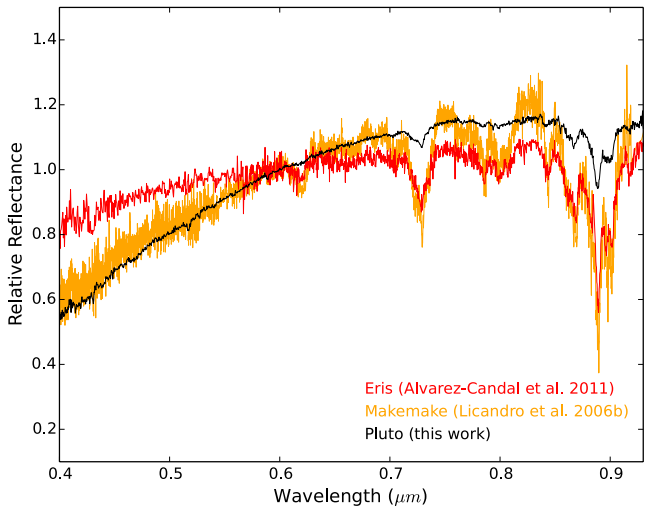

Fig. 4. Comparison of the spectra of Eris, Pluto, and Makemake. The three spectra are normalized at 0.60 μm. All three objects show the absorption bands of methane ice. The band at 0.62 μm is more evident on Makemake and Eris than on Pluto.

straight line to the continuum on both sides of the band between 0.593–0.615 μm and 0.624–0.653 μm and divide the spectrum by this continuum (see Fig. 5). A first look at the plots in Fig. 5 suggests a detection of the band, although in some of the phases (e.g., 49.7° or 103.7°), it is not clear if the absorption is significant above the noise.

We then calculate the area of the absorption band after division by the continuum, integrating it between 0.615 and 0.624 μm. We propagate the errors, taking the error associated with the relative reflectance and the error in the calculation of the fit of the continuum into account in each point. Finally, we iterate the computation of the area, randomly changing the limits of the band, and we take the mean value and the standard deviation as the final values for the area and the associated error. For all the spectra (even those where the detection was suspicious), the integrated area of the band is a positive value. Some of the integrated areas, however, have large uncertainties. To confirm the detection and discard a serendipitous result, we do a second verification.

For this test we repeat the procedure on a region of the continuum where no band is expected. We define this continuum in a region with the same number of points between 0.55 and 0.57 μm. What we can expect from this test is that we obtain both positive and negative values for the area and that the absolute values of the areas are smaller than the uncertainty. In Table 4 we show the results of this test. From the calculation of the integrated area on the region of the continuum, we obtained both positive and negative values, whereas we only obtained positive values from the calculation on the region of the absorption bands at 0.62 μm. After this test, we can consider the detection of the absorption bands at 0.62 μm as reliable, with the phase centered at ~360° as the clearest detection.

3.3. Band depth

To evaluate the globally averaged distribution of CH_4-ice around Pluto's surface, we computed the depth of the absorption bands as $D = 1 - R_b/R_c$, where R_b is the reflectance in the center of

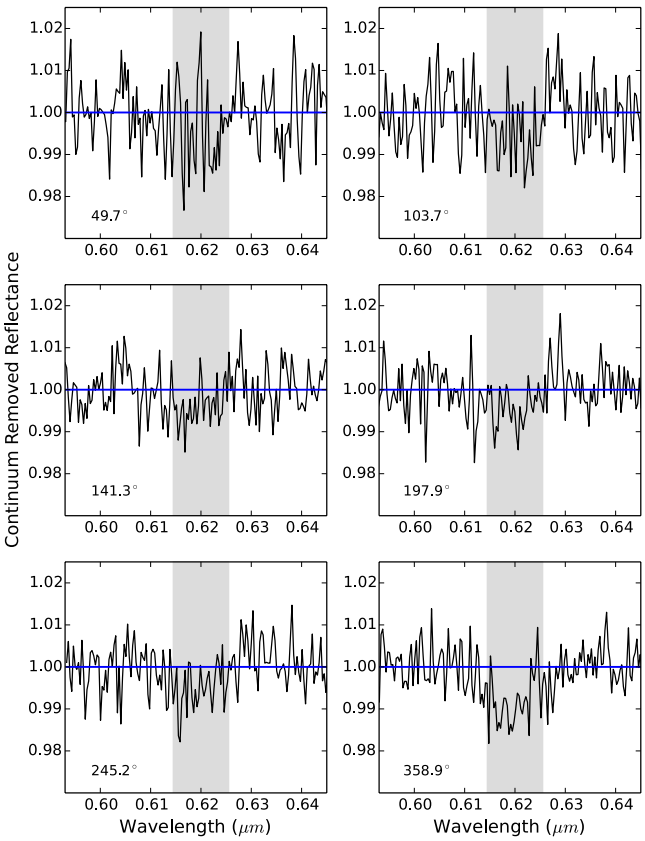

Fig. 5. Continuum removed in the region of the spectra around the 0.62 μm absorption band of methane. The blue line represents the continuum. The gray shadow represents the range of wavelengths used to calculate the area of the bands.

Table 4. Integrated area of the absorption band (in unit of relative reflectance value relative to continuum per microns) at 0.62 μm and test on the continuum between 0.55 and 0.57 μm measured as explained in the text.

Longitude	Band at 0.62 μm ($\times 10^{-4}$)	Cont. 0.55–0.57 μm ($\times 10^{-4}$)
49.7°	0.31 ± 0.30	0.07 ± 0.70
103.7°	0.39 ± 0.21	0.51 ± 0.54
141.3°	0.29 ± 0.13	0.30 ± 0.35
197.9°	0.33 ± 0.14	–0.11 ± 0.41
245.2°	0.37 ± 0.14	0.26 ± 0.46
358.9°	0.66 ± 0.16	–0.57 ± 0.31
Average spectrum	0.35 ± 0.09	0.13 ± 0.17

the band, and R_c the reflectance of the continuum at the same wavelength. Because several of the absorption bands of CH_4 in our spectra are a superposition of different absorption bands, it is not possible to measure the integrated area or the equivalent width of each single band. We calculated the band depth that can be isolated, 0.62, 0.73, 0.79, 0.80, 0.84, 0.87, 0.89, and 0.90 μm, for our six spectra of Pluto. To evaluate the uncertainty in the calculation of the depth, we propagated the errors, taking into account the uncertainties associated both with the value of the relative reflectance in the center of the band and with the value of the continuum at the same wavelength. In Table 5 we list the values obtained for the depths (in %) of the six spectra of Pluto and the corresponding errors.

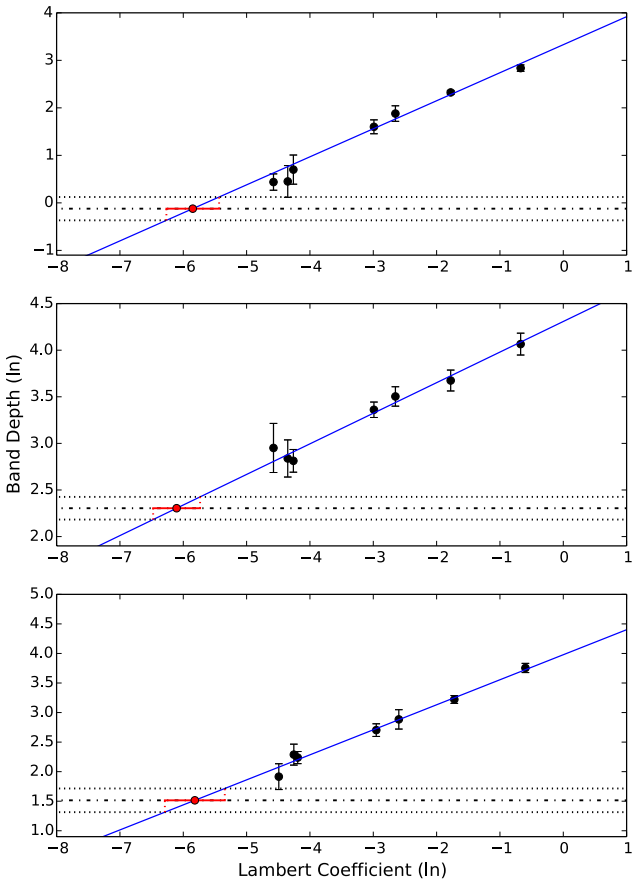

Fig. 6. Band depth (on natural logarithmic scale) vs. Lambert coefficients (on natural logarithmic scale) for Pluto (*top panel*), Makemake (*middle panel*), and Eris (*bottom panel*).

3.4. Lambert coefficients

The appearance of an intrinsically weak band like the one at 0.62 μm shown in Sect. 3.3 demonstrates a very long (several cm) path length of sunlight in the nitrogen ice in which CH_4 is incorporated as a trace constituent. This, in turn, helps to set the size scale for the individual elements of polycrystalline solid N_2 that is characteristic of the surface of Pluto.

A big effort has been made to estimate the absorption coefficients of methane ice by means of laboratory experiments (e.g., Grundy et al. 2002). However, these experiments do not typically cover wavelengths below 0.70 μm, since large slab of methane is needed to produce that absorption. We used this band observed in the spectrum of Pluto, Eris, and Makemake to estimate the absorption coefficient of CH_4 ice at 0.62 μm. For this purpose, we plotted the estimated band depth for the bands in the 0.73–0.90 μm range on a logarithmic scale for the spectra of Pluto (for each band we used the average of the six values obtained for the six spectra) as a function of the corresponding Lambert coefficients at T = 40 K from Grundy et al. (2002). We used the Lambert coefficients for this temperature because the available ones are given in steps of 10 K, and 40 K is closer to the temperature of Pluto. Finally we fit a one-degree polynomial (i.e., straight line) to the points with a least squares fit (see Fig. 6 top panel).

We did the same for the spectrum of Makemake from Licandro et al. (2006b) and for the spectrum of Eris from Alvarez-Candal et al. (2011). In the case of Eris, we used the

Table 5. Band depth (%) and one-sigma errors for eight methane bands at each of the six longitudes observed.

Longitude	0.62 μm	0.73 μm	0.79 μm	0.80 μm	0.84 μm	0.87 μm	0.89 μm	0.90 μm
49.7°	1.16 ± 0.96	4.97 ± 0.74	2.57 ± 1.23	2.52 ± 1.10	1.49 ± 1.63	7.07 ± 1.59	17.35 ± 1.34	10.19 ± 0.81
103.7°	0.89 ± 0.74	4.27 ± 1.03	0.97 ± 0.58	1.12± 0.68	1.54 ± 0.59	5.69 ± 1.64	16.03 ± 1.40	9.98± 0.55
141.3°	0.50 ± 0.48	4.08 ± 0.90	1.33 ± 1.20	1.50 ± 1.04	1.59± 1.56	5.13 ± 1.98	15.77± 2.34	9.85 ± 0.54
197.9°	0.75 ± 0.41	5.16 ± 0.46	0.93± 0.57	1.58 ± 0.53	1.05± 0.46	6.68 ± 2.64	16.74± 1.17	9.89 ± 1.44
245.2°	0.89 ± 0.67	4.99 ± 1.04	1.77± 0.44	2.37 ± 0.71	1.90 ± 1.05	6.28 ± 1.87	17.33± 1.53	11.01± 0.73
358.9°	1.13 ± 0.38	6.29 ± 0.86	1.85 ± 0.86	3.00 ± 0.61	1.75 ± 0.69	8.47 ± 1.49	19.13 ± 1.41	10.41 ± 1.09

Table 6. Band depths (%), with respective errors and Lambert coefficients (Grundy et al. 2002) used for extrapolating the Lambert coefficient at 0.62 μm.

Object	0.62 μm	0.73 μm	0.79 μm	0.80 μm	0.84 μm	0.87 μm	0.89 μm	0.90 μm
Pluto*	0.9 ± 0.3	5.0 ± 0.8	1.6 ± 0.6	2.0 ± 0.7	1.6 ± 0.3	6.6 ± 1.2	17.1 ± 1.2	10.2 ± 0.4
Makemake**	10.0 ± 1.3	28.8 ± 2.5	17.1 ± 3.8	16.7 ± 2.2	19.1 ± 5.8	33.2 ± 3.7	58.3 ± 7.3	39.4 ± 4.7
Lambert Coef. (40 K)	$\mathbf{(2.23 \pm 1.23) \times 10^{-3}}$	5.03×10^{-2}	1.29×10^{-2}	1.41×10^{-2}	1.03×10^{-2}	7.06×10^{-2}	5.10×10^{-1}	1.69×10^{-1}
	$\mathbf{(2.88 \pm 0.85) \times 10^{-3}}$							
Eris**	4.6 ± 1.0	14.9 ± 1.7	9.9 ± 1.9	9.4 ± 1.0	6.8 ± 1.7	17.9 ± 3.2	42.7 ± 3.5	25.1 ± 1.7
Lambert Coef. (30 K)	$\mathbf{(2.97 \pm 1.46) \times 10^{-3}}$	5.22×10^{-2}	1.42×10^{-2}	1.51×10^{-2}	1.12×10^{-2}	7.45×10^{-2}	5.50×10^{-1}	1.79×10^{-1}

Notes. The values of the coefficient for the band at 0.62 μm, in bold format, have been estimated in this work. The upper one for 40 K is calculated using the spectrum of Pluto, and the lower one is calculated using the Makemake spectrum. The value for 30 K is calculated using the spectrum of Eris. The other Lambert coefficients are taken from Grundy et al. (2002). (*) Indicates average of the values computed for the six spectra shown in Table 5; (**) band depth measured for the spectrum of Makemake from Licandro et al. (2006b) and for the spectrum of Eris from Alvarez-Candal et al. (2011).

Lambert coefficients corresponding to $T = 30$ K, because this temperature is more similar to what is estimated for the surface of this object (see Fig. 6 bottom panel). In both cases we measured the band depth of methane ice in the spectrum of Makemake and Eris from the literature following the same procedure described in the previous section for Pluto.

In all the plots in Fig. 6, the blue line is the least squares fit, and the horizontal discontinued line corresponds to the measured band depth at 0.62 μm with its corresponding error (horizontal dotted lines). The intersection between the line fitting the points and the measured band depth value for 0.62 μm band (red point) represents the extrapolated value of the Lambert coefficient for the 0.62 μm band and its error (red line). In Table 6 we listed the band depths (%) with the respective errors and the value of the Lambert coefficient for each band, as taken from the literature.

The value of the extrapolated Lambert coefficients at 0.62 μm for Pluto is $2.88 \times 10^{-3} \pm 1.23 \times 10^{-3}$ cm^{-1}, while the value obtained for Makemake is $2.23 \times 10^{-3} \pm 0.85 \times 10^{-3}$ cm^{-1}. The two values agree within the errors.

The value obtained for Eris is $2.97 \times 10^{-3} \pm 1.46 \times 10^{-3}$ cm^{-1}. The difference due to the temperature is not significant within the error in the calculation.

3.5. Shifts of the center of the bands

The centers of the absorption bands of methane ice provide information about the mixing ratio of methane and nitrogen (Quirico & Schmitt 1997). When methane is diluted in nitrogen ice in small proportions, the centers of the methane bands are shifted toward bluer wavelengths (Quirico & Schmitt 1997), and the shift is greater as the content of nitrogen increases (Brunetto et al. 2008). Some works (Quirico & Schmitt 1997; Quirico et al. 1999; Douté et al. 1999; Merlin et al. 2010) discuss the existence of regions formed of pure CH_4 segregated from the N_2:CH_4 solution. This effect was first reported for Pluto by Owen et al. (1993). However, this conflicts with both alternative models for explaining Pluto's atmosphere. According to Trafton (2015) and references therein, the surface of Pluto is instead covered by a solid solution of these ices, N_2:CH_4, with different mixing ratios. Moreover, two dilution regimes, one saturated in CH_4 and the other saturated in N_2 coexist on the surface of Pluto. The dilution regime saturated in CH_4 is the responsible for the relatively unshifted part of the Pluto's spectra, which was previously attributed to pure CH_4.

We measured the shifts in the center of the bands by comparing our spectra with theoretical relative reflectances of pure methane ice. The synthetic relative reflectances were calculated using a Shkuratov model (Shkuratov et al. 1999) and the optical constants of methane for $T = 40$ K from Grundy et al. (2002).

For comparison, we obtained a suit of relative reflectances considering different grain sizes, then we shifted each model in wavelength until we found the best comparison. We used a chi-square test to choose the best combination of grain size and shift. To evaluate the error associated with the measurement, we repeated the process several times, randomly excluding some points of our spectra and changing the limits of the bands. The obtained shifts are listed in Table 7. In some cases, the low signal-to-noise or to the presence of some artifacts that appear during the reduction process and change the shape of the band means that it has been impossible to measure the band shift.

4. Discussion

Previous works have shown that Pluto presents a surface with a zonal (longitudinal) heterogeneity (Grundy & Fink 1996; Buie et al. 2010a,b; G13). This heterogeneity is clearly seen in processed images of Pluto from the HST (Buie et al. 2010b) and in the recently released images of the New Horizons mission[1].

[1] http:www.nasa.gov/mission_pages/newhorizons

Table 7. Shifts (Å) of the center of the absorption band of CH_4.

Longitude	0.6190 μm	0.7296 μm	0.7862 μm	0.7993 μm	0.8442 μm	0.8691 μm	0.8897 μm	0.9019 μm
49.7°	–	–7.4 ± 4.6	–	–	–	–	–7.6± 1.5	–
103.7°	–	–15.6 ± 2.7	–	–	–9.3 ± 1.7	–13.9 ± 2.2	–13.9 ± 1.8	–
141.3°	–	–	–	–	–	–	–	–
197.9°	–	–12.1 ± 1.4	–	–14.8± 2.5	–6.9 ± 2.7	–10.8 ± 6.3	–15.7 ± 3.4	–
245.2°	–	–5.7 ± 1.8	–	–	–	–5.5 ± 2.6	–	–
358.9°	–	–4.7 ± 2.7	–7.1 ± 2.0	–4.0 ± 3.0	–	–3.1 ± 2.6	–8.8 ± 2.3	–

The heterogeneity is associated with an uneven distribution of the ices (CH_4, N_2, CO) and the complex organics on the surface.

G13 report long time trends in near-infrared spectra obtained between 2000 and 2012 from the analysis of the absorption bands of CH_4, CO, and N_2 present in the spectra. They find that the absorptions of CO and N_2 are concentrated on Pluto's anti-Charon hemisphere (~180°), unlike absorptions of less volatile CH_4 ice that are offset by roughly 90 degrees from the longitude of maximum CO and N_2 absorption. On the time scale of their observations, they find variations in the depth and in the amplitude of the diurnal variation of the absorption bands of CH_4, CO, and N_2. They conclude that the geometric distribution of these ices (in particular CO and N_2) on the surface of Pluto can explain these secular changes, although seasonal volatile transport could be at least partly responsible.

Although visible wavelength spectroscopy does not enable the study of the N_2 and CO concentrations, we can discuss the longitudinal variation within our set of observations and the secular variation when comparing with previous observations of the distribution of methane ice and of the dark-red organic material. Also, from the study of the center of the CH_4 bands, we can extract information on the relative amount of CH_4 diluted in N_2.

With respect to the methane, G13 find that the stronger CH_4 absorption bands have been getting deeper, while the amplitude of their diurnal variation is diminishing, consistent with additional CH_4 absorption at high northern latitudes rotating into view as the sub-Earth latitude moves north. They conclude that the case for a volatile transport contribution to the secular evolution looks strongest for CH_4 ice, despite it being the least volatile of the three ices.

4.1. Longitudinal variations

We note from Fig. 2 that spectra at different longitudes have different albedos, as well as different overall shapes across the full spectral range, demonstrating the longitudinal heterogeneity of the surface of Pluto. To show this in more clearly in Fig. 7, where we plotted the variation with longitude of the spectral slope value obtained from our spectra and compared it with a map of part of the surface of Pluto (mostly the northern hemisphere that is also the hemisphere currently observed from Earth) obtained by the New Horizons mission[2]). The highest (redder) value of the slope (at longitude ~100°) is centered on the hemisphere that, according to the new maps of Pluto, contains the large dark region, whereas lower values correspond to a zone that is on average brighter (~240°). This is compatible with a higher abundance of solid organic material (redder in color and lower in albedo than the icy species observed in Pluto) in the darker region and a higher abundance of ices in the brighter ones.

In Fig. 8 (bottom panel), we show the variation in the band depth of the five stronger CH_4 absorption bands measured in our spectra. A sinusoidal trend is clearly visible with a minimum at a longitude between 140°–160° and a maximum at a longitude near 360°. This phase (360°) is also the one with the clearest detection of the 0.62-μm band. The location of this CH_4 maximum agrees with the trend found by G13 (maximum CH_4 between 260° and 320°), but appears a bit shifted to the east. In particular, G13 finds that there are subtle differences in the longitude of the maximum of the absorption for different bands of CH_4, with the weaker absorption bands having the minimum and maximum at longitudes more to the east than the stronger CH_4 absorption bands (see Fig. 4 of G13). They interpret this difference between stronger and weaker bands as due to the presence of different terrain types, with terrains with larger particles or with greater CH_4 enrichment, that produce the weaker bands that are more prevalent on the Charon-facing hemisphere. Figure 8 shows how this trend continues for the bands in the visible that are even weaker than in the NIR, with the shallowest bands (0.80 and 0.79 μm) having a minimum at ~180° and a maximum at ~360°. The largest abundance of CH_4, or the largest particles, can be found in the hemisphere centered at ~0°, and is not coupled with either the darkest (probably higher organic abundance) or the brightest areas (probably higher volatile component).

With respect to the degree of dilution of CH_4 in N_2, G13 found that all the CH_4 bands in the infrared range show a blue shift (indicative of dilution) with a minimum blue shift corresponding to the Charon-facing hemisphere and a maximum blue shift corresponding to the anti-Charon hemisphere. That is exactly what Fig. 9 shows, with a maximum absolute value of the shifts between 100° and 200° of longitude, corresponding to the anti-Charon hemisphere. The minimum of the shifts corresponds to a region where the abundance of methane is higher (the Charon-facing hemisphere). This could indicate a higher degree of saturation of CH_4 in this hemisphere (Tegler et al. 2012; Grundy et al. 2013; Trafton 2015). Our measurements in the visible show the same trend as do the estimates from the NIR observations, apparently indicating that the degree of dilution is uniform over different path lengths of the light.

4.2. Secular variations

To compare our observations with earlier spectral data, we show all our spectra in Fig. 10, with spectra from Buie & Fink (1987) and Grundy & Fink (1996) overplotted on spectra obtained at similar longitudes (but more northern latitudes). For example, we compare our spectrum taken at a longitude of 49.7° (sub-Earth latitude 51°) with Grundy and Fink's data for 1993 (longitude 56°, sub-Earth latitude ~11°), and our spectrum at 358.9° longitude (sub-Earth latitude 51°) with 1983 spectrum from Buie & Fink (1987) (longitude 329°, sub-Earth latitude ~–10°). Differences in the new spectra compared to earlier data can be

[2] http://www.nasa.gov/mission_pages/newhorizons

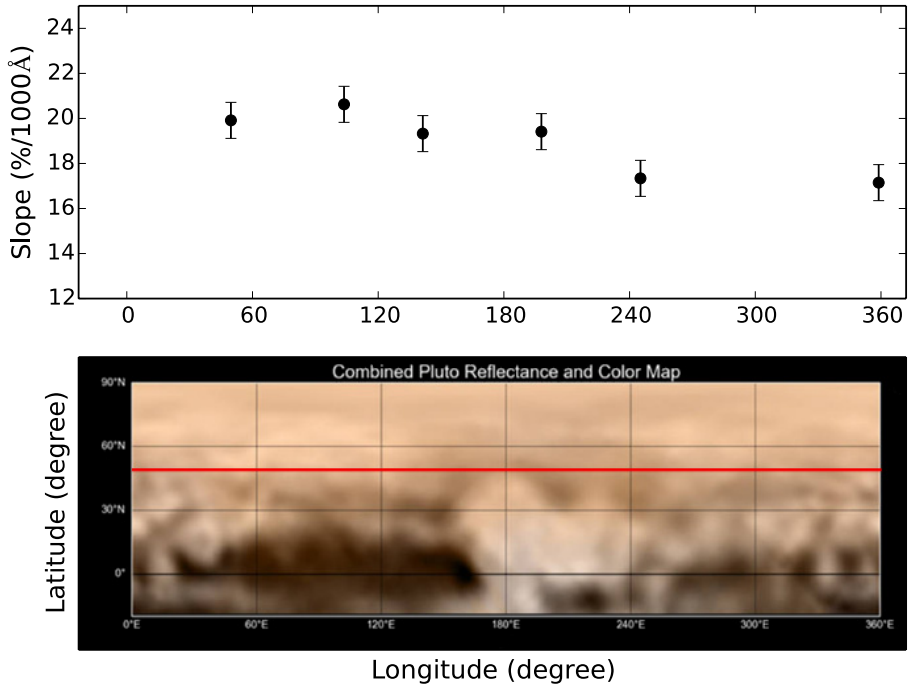

Fig. 7. Spectral slope (%/1000 Å), calculated between 0.40 and 0.75 μm for spectra of Pluto normalized at 0.60 μm vs. longitudes (*top panel*), and map of part of the surface of Pluto result of combination of images taken by the Long Range Reconnaissance Imager (LORRI) on New Horizons and combined with the lower-resolution color data from the instrument Ralph on the spacecraft (*bottom panel*) (http://www.nasa.gov/mission_pages/newhorizons). The scale of the horizontal axis is the same for the *top and bottom panels*. The red line indicates the sub-Earth latitude at which our data have been obtained (~51°).

a result of the different latitude aspects, temporal changes, or a combination of both. From the comparison of the slopes in the visible (see Table 3), we can see that the spectra obtained in 2014 are all redder than corresponding previous spectra. This could suggest a stronger presence of complex organics on Pluto's surface with respect to previous epochs.

G13 reported a difference in the secular evolution between stronger and weaker methane absorption bands observed in the near-infrared. Grundy & Fink (1996) and G13 attribute this to a different evolution of CH_4 poor terrains (that only produce the stronger bands) and of terrains richer in CH_4 (that produce the weaker bands). They find that the stronger bands increase in strength with years, while the weaker bands in their sample do not. If this trend extends to the visible wavelengths as already noted by Grundy & Fink (1996), we would see a secular decrease in the depth of the bands. Indeed, from Fig. 11, we can note that the depths of the bands at 0.73 and 0.89 μm measured in our spectra are lower than those reported in Grundy & Fink (1996).

G13 also find that the amplitude of the pattern of the longitudinal variation decreases with time. This is consistent with the change over the years of the sub-Earth latitude of Pluto, with an increasing contribution to the observed spectrum of northern polar ices over the contributions from equatorial and southern latitudes, which as seen in the color map in Fig. 7, show a much greater contrast with longitude. In Fig. 11 (top and middle panels), we plotted the measured band depth of the weak bands at 0.73 and 0.89 μm, along with the depth of the same bands from Grundy & Fink (1996), and a sinusoidal fit for each data set. In the bottom panel we show, for comparison purposes, the secular variation of the strong band at 1.72 μm from G13. The depths and the amplitude of the variations measured by us are slightly lower than those of 1983–1994, following the same trend of the near-infrared bands described in G13.

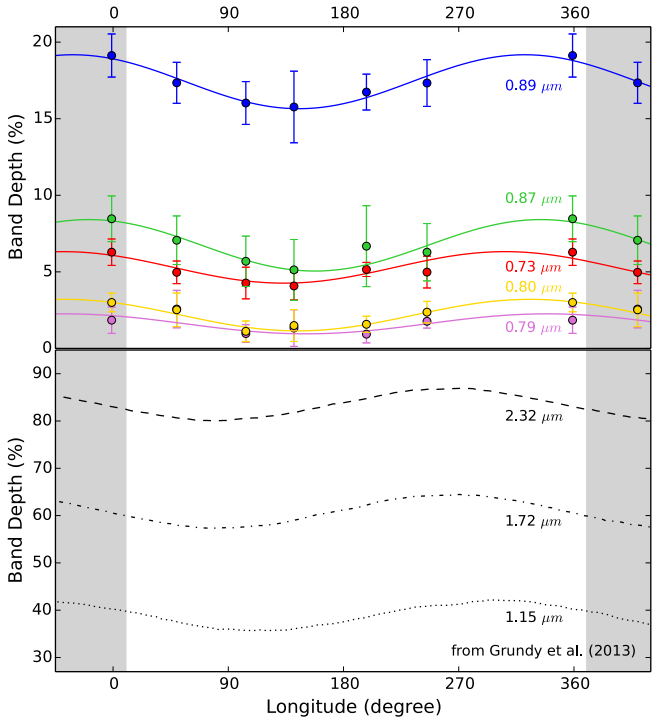

Fig. 8. *Top panel*: variation in the band depth (in %) with longitude for the five stronger CH_4 absorption bands measured from the spectra of Pluto presented in this work. *Bottom panel*: variation in the depth of the absorption bands at 1.14, 1.72, and 2.32 μm from G13. The points in the gray shadow represent replicate values (at longitude ± 360°) to better visualize the variation in the band depth with the longitude.

It is good to keep in mind that because Pluto has not been observed over a whole orbit, it is especially difficult to characterize

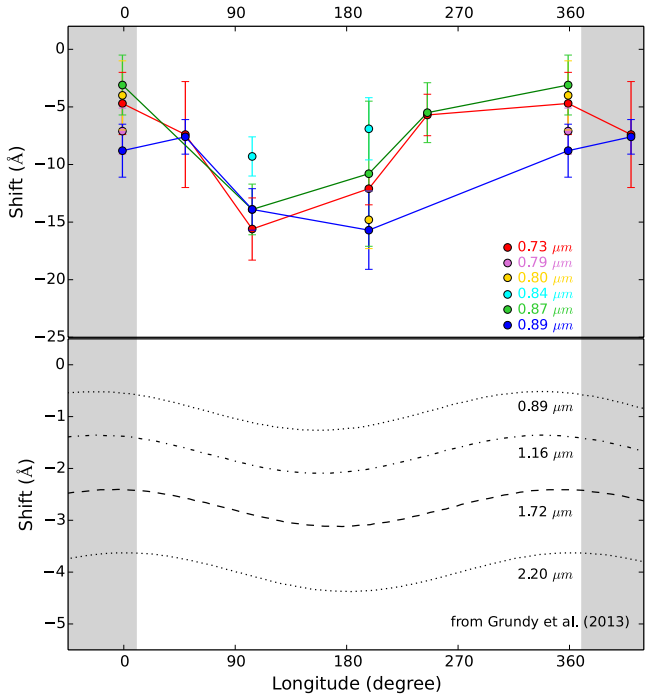

Fig. 9. *Top panel*: measured band shifts (Å), with respect to the position of the pure methane from this work vs. Pluto's longitude. We connected the points corresponding to the bands at 0.73, 0.87, and 0.89 μm with lines to illustrate the variation with longitude (for the other bands, there are too few points). At longitudes between 100° and 200°, the shifts are greater, thus the CH_4:N_2 is smaller, which is compatible with a lower abundance of CH_4 suggested by the smaller band depths shown in Fig. 8. *Bottom panel*: variation in the shifts (Å) of the bands at 0.89, 1.16, 1.72, and 2.20 μm with respect to the position of the pure methane, from G13. The points in the gray shadow represent replicate values (at longitude ±360°) to better visualize the variation in the band depth with the longitude.

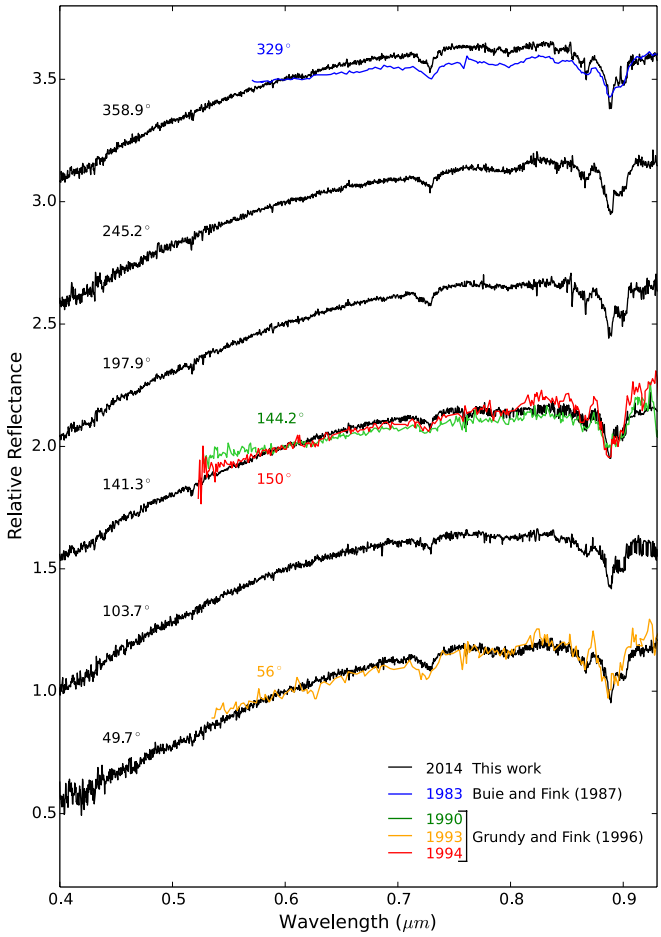

Fig. 10. Secular variation on Pluto reflectance. Pluto-Charon spectra from this work shown with data at similar spectral resolution and signal precision from Buie & Fink (1987) and Grundy & Fink (1996) at similar longitudes. All the spectra are normalized at 0.60 μm and shifted by 0.5 in relative reflectance for clarity.

secular variations, since they might be confused with seasonal or regional (geometrical) variations. The analysis of the secular variation of the slope in the visible shows a reddening of Pluto's surface from 1983 to 2014, suggesting a higher degree of processing of the surface. On the other hand, the analysis of the secular variation of the methane ice bands in the visible is consistent with the results from the NIR and indicates a decrease in the contrasts in band depth along Pluto's surface. In our case, the clear correspondence of these changes with the pattern seen in the color maps of Pluto obtained with New Horizons supports the contention that they are probably dominated by the sub-Earth latitudinal change rather than by seasonal changes.

4.3. Comparison with Makemake and Eris

To compare the spectral properties of Pluto, Makemake, and Eris, in Sect. 3 we calculate slope and band depths for both the same parameters as computed for Pluto's spectra.

The spectral slope of Pluto calculated between 0.57 and 0.70 μm is identical within the errors to that of Makemake from Licandro et al. (2006b) and three times larger than the spectral slope of Eris from Alvarez-Candal et al. (2011) (see Table 3 and Fig. 4). This suggests that the surface of Makemake contains a similar amount of solid complex organics (the coloring agent) as Pluto (averaging over the entire surface), while Eris's surface has a smaller amount of organics than both Pluto's and Makemake's, as previously suggested (e.g., by Lorenzi et al. 2015, and references therein). This shallower spectral slope is consistent with refreshing of the surface of Eris with volatile ices (N_2, CO, CH_4) deposited after the collapse of the atmosphere at some intermediate distance on Eris' way from aphelion to the perihelion, as suggested by Licandro et al. (2006a) and Alvarez-Candal et al. (2011).

On the other hand, the methane bands are consistently deeper in the Makemake spectrum than in the Eris spectrum, and in the Pluto spectrum they are even weaker (see Table 6 and Fig. 4). This indicates that methane is more abundant on the surface of Makemake than on Eris, and on the surface of Eris than on Pluto, as previously reported by Licandro et al. (2006b).

4.4. Other applications

The spectra presented in this paper provide an independent calibration of the MVIC (Multispectral Visible Imaging Camera) instrument (Reuter et al. 2008) aboard the New Horizons spacecraft, and allow synthesis of a "green channel" that enables the preparation of false-color images of Pluto with the data from the spacecraft encounter. Figure 12 shows an average spectrum of Pluto from the present investigation with the transmission curves of the MVIC filters superimposed. Overplotted we show the photometric appearance of this spectrum as seen through MVIC

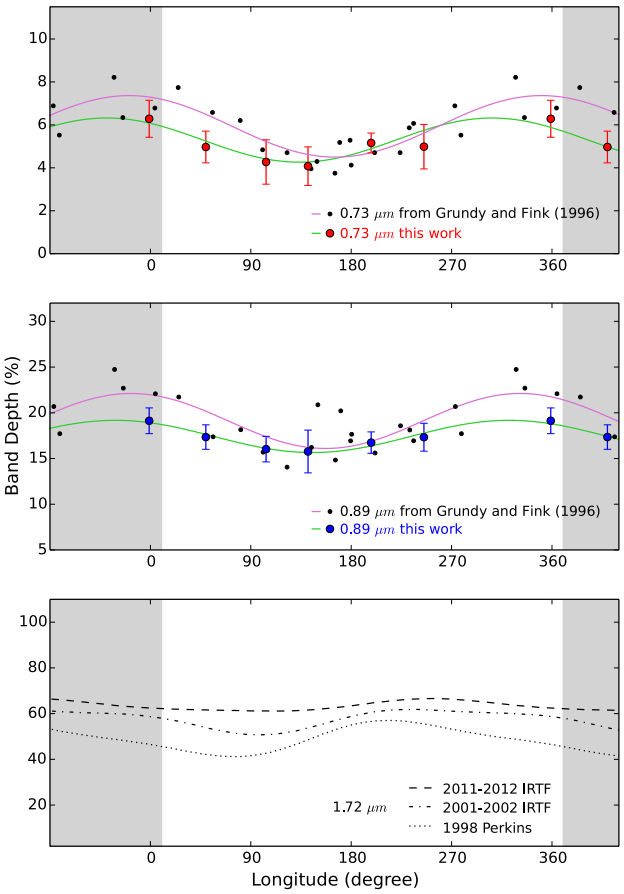

Fig. 11. Secular trend of the methane absorption bands: variation in the absorption band depth for the bands at 0.73 μm (*top panel*) and 0.89 μm (*middle panel*) compared with the secular variation for the band at 1.72 μm (*bottom panel*) from G13. Lines in green represent a sinusoidal fit of band depths from this work; lines in purple represent a sinusoidal fit of band depths from Grundy & Fink (1996). The points in the gray shadow represent replicate values (at longitude 360°) to better visualize the variation in the shifts with the longitude.

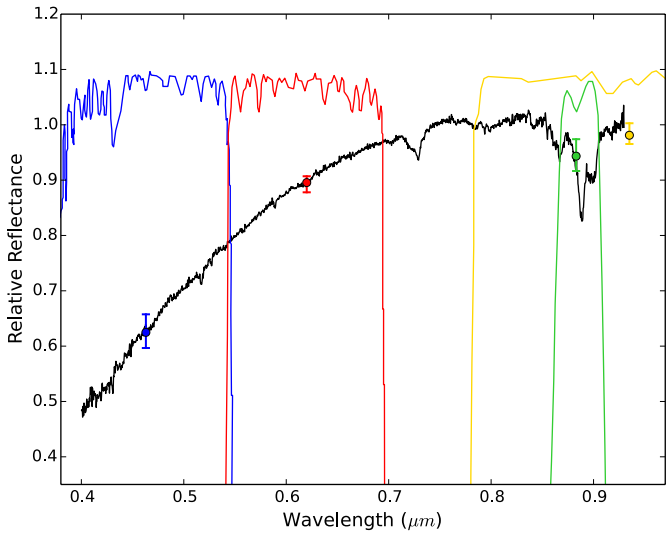

Fig. 12. Longitudinal variation inferred for MVICS observations. The average spectrum from the 2014 observations presented in this work is presented with the filter transmission bands of the New Horizons Multispectral Visible Imaging Camera (MVIC; Reuter et al. 2008). The colored dots show the convolution of these transmissions with the average Pluto spectrum. The vertical bar shows the variation among the six reflectances (maximum and minimum values). The value at the NIR band is a lower limit since our spectra do not cover the full band pass of that filter.

filters. The vertical lines indicate the maximum and minimum values of these "convolved photometric" points from our set of spectra and give an indication of how the variation showed by our data could be detected by MVIC.

These new spectra provide the desired color information for modeling efforts that will use optical constants for non-ice materials presently being synthesized in the laboratory by the UV and electron-irradiation of a Pluto mixture of ices known from near-IR spectroscopy (N_2:CH_4:CO, 100:1:1). The chemical analysis of the refractory residue from a UV-irradiated Pluto ice mixture has been published by Materese et al. (2014), and results from the electron-irradiated ices are presented in Materese et al. (2015).

5. Conclusions

Low-resolution visible spectra of Pluto at six different planetocentric longitudes between May 13 and July 17, 2014 were obtained using the ACAM imager/spectrograph of the 4.2 m *William Herschel* Telescope (Observatorio del Roque de los Muchachos, La Palma, Spain). These data cover a whole rotation of Pluto with a step of ~50° and a gap at ~300°.

The new spectra clearly show methane ice absorption bands at 0.73, 0.78–0.80 μm, and 0.83–0.91 μm also seen in previously reported spectra of Pluto (Grundy & Fink 1996). We reported the detection of the spectra of the methane-ice band equivalent of the 0.62-μm CH_4 gas absorption band in Pluto spectrum. This band was previously reported in the spectra of TNOs Eris and Makemake (Alvarez-Candal et al. 2011; Licandro et al. 2006b). The measurement of the depth of the absorption band of methane ice at 0.62 μm in the new six spectra of Pluto allowed us to estimate the Lambert coefficient at this wavelength at T = 40 K (not measured in the laboratory yet) as $2.88 \times 10^{-3} \pm 1.23 \times 10^{-3}$ cm^{-1}. From the Makemake spectrum, we obtained a similar value within errors, $2.23 \times 10^{-3} \pm 0.85 \times 10^{-3}$ cm^{-1}. From the spectrum of Eris, we obtained a Lambert coefficient of $2.97 \times 10^{-3} \pm 1.46 \times 10^{-3}$ cm^{-1}, in this case for a T = 30 K.

The spectral properties of Pluto, compared to those of Makemake and Eris, support that Pluto's surface holds a similar amount of solid complex organics (the coloring agent) as Makemake, while Eris's surface has a lesser amount of organics than them both, as previously suggested (e.g., Licandro et al. 2006b; Alvarez-Candal et al. 2011; Lorenzi et al. 2015). On the other hand, our spectra confirm that methane is less abundant in the Pluto's surface than on those of Eris and Makemake, as previously reported by Licandro et al. (2006b).

The longitudinal variation of the slope in the visible is in phase with the distribution of the dark and bright material as seen in the color maps of Pluto from New Horizons, with the reddest slopes in the hemisphere centered at 90° and the less red material in the hemisphere centered at 270°.

The longitudinal and secular variations of the methane bands observed in the visible wavelengths are consistent with the behavior of the weak absorption bands in the near-infrared region reported by G13. The maximum absorption due to methane ice is located at the phase centered at 360° (Charon-facing hemisphere) and the minimum at ~180° (anti-Charon-facing

hemisphere). The curve is shifted from the curves of the stronger methane ice bands in the NIR. The depths and the amplitude of the diurnal variations of the methane ice in the spectra presented here (54° N) are slightly lower than those of 1983–1994 (Grundy & Fink 1996), following the same trend of the near-infrared bands as described in G13. This trend indicates that our observations capture regions with a lower contrast and agrees with the contrast in the color maps of Pluto with more dark and bright material lying in the equatorial latitudes.

All of the detected CH_4 bands are blueshifted with respect to the position for pure methane ice, indicating a certain degree of dilution of the CH_4 in other ice, probably N_2. We observed a longitudinal variation with a maximum shift located at longitudes between 100°–200° and a minimum shift around 360° longitude. That the shift is minimum in the regions where the abundance of methane is higher could be indicative of a dilution of CH_4:N_2 that is more saturated in CH_4.

Acknowledgements. This paper is based on data from override observations made with the *William Herschel* Telescope, under program 055-WHT11/14A, operated on the island of La Palma by the Isaac Newton Group in the Spanish Observatorio del Roque de los Muchachos of the Instituto de Astrofísica de Canarias. D.P.C., W.M.G., and R.P.B. were supported in part by NASA's New Horizons mission. J.L. acknowledges support from the project ESP2013-47816-C4-2-P (MINECO, Spanish Ministry of Economy and Competitiveness). We want to thank the referee E. Lellouch for his valuable comments that improved the manuscript.

References

Alvarez-Candal, A., Pinilla-Alonso, N., Licandro, J., et al. 2011, A&A, 532, A130
Barker, E. S., Cochran, W. D., & Cochran, A. L. 1980, Icarus, 44, 43
Bell, J. F., Clark, R. N., McCord, T. B., & Cruikshank, D. P. 1979, in BAAS, 11, 570
Benn, C., Dee, K., & Agócs, T. 2008, in SPIE Conf. Ser., 7014, 6
Benner, D. C., Fink, U., & Cromwell, R. H. 1978, Icarus, 36, 82
Binzel, R. P. 1988, Science, 241, 1070
Brunetto, R., Caniglia, G., Baratta, G. A., & Palumbo, M. E. 2008, ApJ, 686, 1480
Buie, M. W., & Fink, U. 1987, Icarus, 70, 483
Buie, M. W., Grundy, W. M., Young, E. F., Young, L. A., & Stern, S. A. 2010a, AJ, 139, 1117
Buie, M. W., Grundy, W. M., Young, E. F., Young, L. A., & Stern, S. A. 2010b, AJ, 139, 1128
Capaccioni, F., Coradini, A., Filacchione, G., et al. 2015, Science, 347, 0628
Cruikshank, D. P., Imanaka, H., & Dalle Ore, C. M. 2005, Adv. Space Res., 36, 178
Cruikshank, D. P., Wegryn, E., Dalle Ore, C. M., et al. 2008, Icarus, 193, 334
Cruikshank, D. P., Dalle Ore, C. M., Clark, R. N., & Pendleton, Y. J. 2014, Icarus, 233, 306
Cruikshank, D. P., Grundy, W. M., DeMeo, F. E., et al. 2015, Icarus, 246, 82
Douté, S., Schmitt, B., Quirico, E., et al. 1999, Icarus, 142, 421
Fix, J. D., Neff, J. S., & Kelsey, L. A. 1970, AJ, 75, 895
Goesmann, F., Rosenbauer, H., Bredehöft, J. H., et al. 2015, Science, 349, 020689
Grundy, W. M., & Fink, U. 1996, Icarus, 124, 329
Grundy, W. M., Schmitt, B., & Quirico, E. 2002, Icarus, 155, 486
Grundy, W. M., Olkin, C. B., Young, L. A., Buie, M. W., & Young, E. F. 2013, Icarus, 223, 710
Imanaka, H., Cruikshank, D. P., Khare, B. N., & McKay, C. P. 2012, Icarus, 218, 247
Khare, B. N., Sagan, C., Arakawa, E. T., et al. 1984, Icarus, 60, 127
King, D. L. 1985, RGO/La Palma technical note no. 31, Tech. Rep.
Landolt, A. U. 1992, AJ, 104, 340
Lazzaro, D., Angeli, C. A., Carvano, J. M., et al. 2004, Icarus, 172, 179
Lellouch, E., de Bergh, C., Sicardy, B., et al. 2015, Icarus, 246, 268
Licandro, J., Campins, H., Hergenrother, C., & Lara, L. M. 2003, A&A, 398, L45
Licandro, J., Grundy, W. M., Pinilla-Alonso, N., & Leisy, P. 2006a, A&A, 458, L5
Licandro, J., Pinilla-Alonso, N., Pedani, M., et al. 2006b, A&A, 445, L35
Licandro, J., Campins, H., Kelley, M., et al. 2011, A&A, 525, A34
Lorenzi, V., Pinilla-Alonso, N., Licandro, J., Dalle Ore, C. M., & Emery, J. P. 2014, A&A, 562, A85
Lorenzi, V., Pinilla-Alonso, N., & Licandro, J. 2015, A&A, 577, A86
Materese, C. K., Cruikshank, D. P., Sandford, S. A., et al. 2014, ApJ, 788, 111
Materese, C. K., Cruikshank, D. P., Sandford, S. A., Imanaka, H., & Nuevo, M. 2015, ApJ, 812, 150
Merlin, F., Barucci, M. A., de Bergh, C., et al. 2010, Icarus, 210, 930
Owen, T. C., Roush, T. L., Cruikshank, D. P., et al. 1993, Science, 261, 745
Pinilla-Alonso, N., de León, J., Walsh, K. J., et al. 2015, A&A, submitted
Quirico, E., & Schmitt, B. 1997, Icarus, 127, 354
Quirico, E., Douté, S., Schmitt, B., et al. 1999, Icarus, 139, 159
Reuter, D. C., Stern, S. A., Scherrer, J., et al. 2008, Space Sci. Rev., 140, 129
Rivkin, A. S., & Emery, J. P. 2010, Nature, 464, 1322
Shkuratov, Y., Starukhina, L., Hoffmann, H., & Arnold, G. 1999, Icarus, 137, 235
Stern, S. A., Bagenal, F., Ennico, K., et al. 2015, Science, 350, 1815
Tegler, S. C., Grundy, W. M., Olkin, C. B., et al. 2012, ApJ, 751, 76
Tholen, D. J., & Buie, M. W. 1990, in BAAS 22, 1129
Tody, D. 1993, in Astronomical Data Analysis Software and Systems II, eds. R. J. Hanisch, R. J. V. Brissenden, & J. Barnes, ASP Conf. Ser., 52, 173
Trafton, L. M. 2015, Icarus, 246, 197
Wright, I. P., Sheridan, S., Barber, S. J., et al. 2015, Science, 349, 020673